ARTICLE

Lithium Intercalation Edge Effects and Doping Implications for Graphite Anodes

Received 00th January 20xx,
Accepted 00th January 20xx

DOI: 10.1039/x0xx00000x

Chao Peng, *[a,d,†] Michael P. Mercer,[b,d,†] Chris-Kriton Skylaris[c,d] and Denis Kramer*[a,d,e]

The interface between the electrolyte and graphite anodes plays an important role for lithium (Li) intercalation and has significant impact on the charging/discharging performance of Lithium-Ion Batteries (LIBs). However, atomistic understanding of interface effects that would allow the interface to be rationally optimized for application needs is largely missing. Here we comprehensively study the energetics of Li intercalation near the main non-basal surfaces of graphite, namely the armchair and zigzag edges. We find that edge sites at both surfaces bind Li more strongly than in the bulk of graphite. Therefore, lithiation of these sites is expected to proceed at higher voltages than in the bulk. Furthermore, this effect is significantly more pronounced at the zigzag edge compared to the armchair edge due to its unique electronic structure. The "peculiar" topologically stabilized electronic surface state found at zigzag edges strongly interacts with Li; thereby changing Li diffusion behavior at the surface as well. Finally, we investigate boron (B)/nitrogen (N) doping as a promising strategy to tune the Li intercalation behavior at both edge systems which could lead to enhanced intercalation kinetics in B/N doped graphite anodes.

Introduction

Due to the significant progress of lithium-ion batteries (LIBs) over the past decades, commercial LIBs are widely applied in electric devices and stand to revolutionise the automotive industry.[1-6] However, while research has produced a variety of viable positive electrode materials, graphite remains the most often employed negative electrode material, because of high capacity, long cycle life, low operating voltage and improved safety.

The use of graphite as negative electrode for rechargeable electrochemical power sources was already suggested by Rudorff and Hofmann in 1938,[7] and first commercially introduced by Sony in 1991.[8] The lithiation of graphite leads to the formation of a series of graphite intercalation compounds (GICs), consisting of periodic arrangements of lithium containing and unoccupied layers in the basal plane of the hexagonal graphite lattice. The "stage" index n (i.e., the number of graphite layers between adjacent intercalated layers such as stage I (LiC_6) and II (LiC_{12}))[9,10] is usually used to denote different GICs. Furthermore, different stages show different kinds of carbon stacking. Prior to lithiation, graphite shows an AB hexagonal stacking, while fully lithiated graphite (LiC_6) shows an AA stacking where Li occupies sites in between the carbon planes above the center of hexagons (see Figure S1).[9,11,12] The Li migration behaviour plays a significant role in the staged (de)lithiation of graphite and is a key factor determining the rate capabilities of LIBs and thus has been widely studied.[12-15]

Lithium diffusion in LIBs is important for battery performance. Using a Devanathan-Stachurski cell and First-Principles calculations, Persson et al. quantified the Li diffusion coefficient in highly oriented pyrolytic graphite (HOPG). They found that Li prefers to diffuse in between graphene layers rather than along the grain boundaries or in the direction perpendicular to the graphene sheets.[16] This trend is valid for all Li concentrations: a much higher diffusion barrier (around 8 eV) exists for Li across the graphene layers than along the (001) graphene plane (below 0.5 eV).[17] However, the Li diffusion coefficient was found to be sensitive to the interlayer spacing at dilute Li concentrations, while at high Li content the in-plane Li-Li interactions appear dominant.[18]

Interestingly, theoretical calculations suggest that Li diffusion is very fast in bulk graphite and only moderately decreases with increasing Li concentration.[18-20] However, this is inconsistent with the reported wide range of effective Li diffusivities (10^{-6} ~10^{-14} cm^2/s) obtained experimentally.[21-23] While the wide range of experimentally reported effective diffusion coefficients is likely to be related to the high anisotropy of the layered material,[22] a deeper understanding of the intercalation behavior is nonetheless desirable in order to rationally optimize graphite electrodes for high rate applications, especially at low temperatures where the necessary large overpotentials increase the risk of Li plating.[24,25] Besides, understanding of the Li diffusion behaviour, not only in

[a] School of Engineering, University of Southampton, Southampton SO17 1BJ, U. K. E-mail: D.Kramer@soton.ac.uk
[b] Department of Chemistry, Lancaster University, Bailrigg, Lancaster, LA1 4YB, U. K.
[c] School of Chemistry, University of Southampton, Southampton SO17 1BJ, U. K.
[d] The Faraday Institution, Quad One, Becquerel Avenue, Harwell Campus, Didcot, OX11 0RA, U. K.
[e] Faculty of Mechanical Engineering, Helmut-Schmidt University, Hamburg, 22043, Germany
† These authors contributed equally.
Electronic Supplementary Information (ESI) available: [details of any supplementary information available should be included here]. See DOI: 10.1039/x0xx00000x

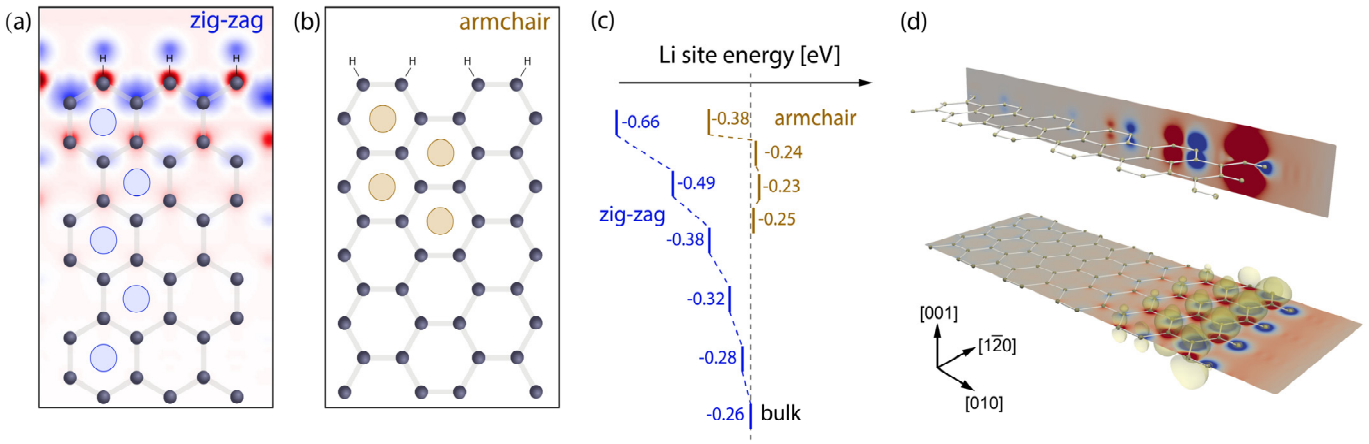

Figure 1. Geometrical structures of graphite edges for zigzag-edged graphite (a) and armchair-edged graphite (b). Periodic boundary conditions were applied in all three directions. (c) is the profile of Li adsorption energies as a function of distance from the edge towards the bulk of graphite. (d) illustrates the spin densities in zigzag-edged graphite. The iso-surface value is 0.0002 e/Å^3.

the bulk but also across the interface between electrolyte and electrode, is fundamental to rationally enhance charge/discharge rates and mitigate the risk of Li plating. However, the field has so far focused on bulk mobility,[16,19,20,26] and the interfaces have attracted relatively little attention, especially at the atomistic level.

Here we investigate the energetics of Li intercalation close to the non-basal edges of graphite, which is markedly different from the bulk due to geometric as well as subtle electronic effects. As Li has to diffuse through these edges due to the prohibitive diffusion barrier across the graphene layers, the Li intercalation behaviour is likely to be influenced by these edge effects.[27,28] Nonetheless, the consideration of edge effects is largely missing in the literature to the best of our knowledge, with rather more work focusing on Li adsorption at the basal plane,[29-31] which is of less relevance for intercalation into graphite than the edge sites. Furthermore, there are currently no widely accepted guidelines for designing carbon-based electrode architectures for lithium ion batteries, especially for high-power applications. In contrast, well-controlled structure and performance-oriented design of cathode materials has recently been explored.[32,33] Therefore, in a first step towards an atomistic understanding of Li intercalation into graphite beyond the bulk, we quantify here the effect of graphite edges on Li diffusion properties and outline possible materials design strategies to increase the rate performance of graphite.

2. Computational details

Theoretical Method. We performed spin-polarized Density-Functional-Theory (DFT) calculations using the Vienna Ab-Initio Simulation Package (VASP). The Perdew-Burke-Ernzerhof (PBE) functional within the generalized gradient approximation has been used throughout.[34-36] The projector-augmented wave method was used to represent the core electrons.[37,38] The valence electronic states were expanded in plane-wave basis sets with cutoff energies of 450 eV. The climbing-image nudged elastic band (NEB) method was employed to search for the transition states of the migration processes, with five images considered between the initial and final state. [39,40] In all cases, the saddle point is characterised by Li located on the border between two hexagons. The force convergence criterion in structural optimization was set to be 0.03 eV/Å. We used a k-mesh of (8×8×8) to optimize the geometry of bulk graphite. For the armchair-edged system, a k-mesh of (2×3×1) was used to sample in Brillouin zone, while a k-mesh of (1×2×1) was used in the zigzag-edged system. For density of states calculations, a (4×6×1) k-point mesh was used. The DFT-D3 method was employed to describe Van der Waals interactions,[41,42] which yields relaxed geometries consistent with experimental lattice constants of pristine graphite (see Table S1).[17]

Structural Model. Slabs were cut from fully relaxed bulk graphite with an AA stacking to construct periodic models of the armchair and zigzag edges (see Figure 1, a and b). Specifically, a *p*(2×4) hydrogen-terminated armchair-edged graphite (a= 13.76 Å, b = 8.53 Å, c = 27.25 Å; α= β= γ= 90°) and a *p*(4×4) hydrogen-terminated zigzag-edged graphite (a= 13.76 Å, b = 9.86 Å, c = 46.98 Å; α= β= γ= 90°) with four graphene layers were constructed, respectively. A vacuum layer of 10 Å was used to minimise interactions between periodic images as shown in Figure S2. Periodic boundary conditions were applied in all 3 directions. All atoms were relaxed during geometrical optimization, while the simulation cell was kept at a geometry commensurate with the fully relaxed bulk.

Adsorption Energies. The adsorption energy of Li is defined as

$$E_{ads} = E(Li|G) - \{E(G) + E(Li)\} \quad (1)$$

where *E*(Li|G), *E*(G) and *E*(Li) represent the total energy of graphite slab containing one Li atom, the equivalent pristine graphite slab with AA stacking and bulk bcc metallic lithium, respectively. We also constructed different sizes of supercells to calculate the adsorption energies of Li in the center of the slabs, as defined in equation (1), to confirm that the Li adsorption energies are consistent with bulk graphite in AA stacking (see Supporting Information).

3. Results and discussion

3.1 Li adsorption in edged graphite

When Li intercalates in graphite, there are three possible sites for Li adsorption in-between graphene layers, namely the top, bridge and hollow sites (see Figure S3). The hollow site is the most stable site for Li adsorption with a bulk adsorption energy of -0.26 eV relative to metallic Li, consistent with other reports.[17,43] It is much lower than Li adsorption at the bridge site (0.20 eV) and the top site (0.19 eV). Therefore, we focus on the hollow sites as the adsorption site for Li.

Figure 1c shows Li adsorption energies from the edge to the bulk in both armchair-edged and zigzag-edged graphite. In the armchair system, the adsorption energy of Li is the largest (i.e., most negative site energy) at the edge site (-0.38 eV) and then decreases rapidly to -0.24 eV in the first sub-surface site, effectively approaching the bulk value of -0.26 eV. The armchair edge, therefore, provides a beneficial Li adsorption site directly at the edge with an 0.12 eV larger adsorption energy relative to bulk graphite.

The Li adsorption energetics near the zigzag edge are markedly different. Li is strongly stabilized near the zigzag edge: the adsorption energy in the edge site is -0.66 eV, almost 0.3 eV larger in magnitude than that calculated for the armchair edge and 0.4 eV larger than in the bulk. Interestingly, surface effects at the zigzag edge are not only stronger, they also penetrate much deeper into the bulk than the edge effects at the armchair edge. Li adsorption energies decease in magnitude from the edge to the bulk more gradually than for the armchair edge, with bulk-like properties reached only in the fifth or sixth sub-surface site.

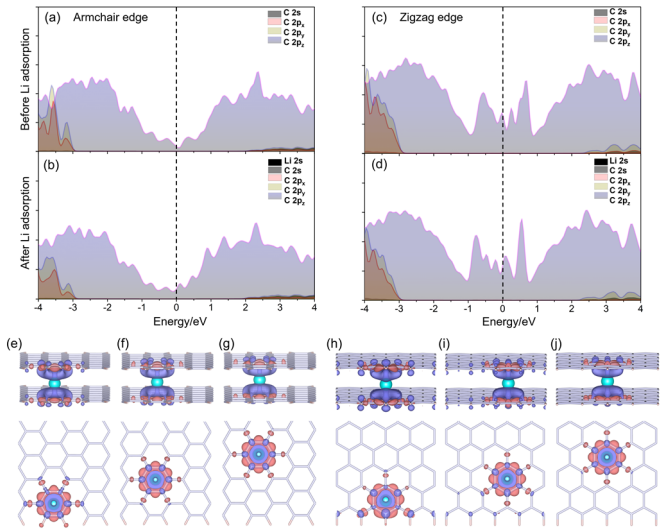

Figure 2. Local density of states (LDOSs) and charge difference of Li adsorption at armchair and zigzag edges. (a) and (b) are LDOSs of edge carbons at armchair edges before and after Li adsorption. LDOSs are projected on the first carbon hexagons at the armchair and zigzag edges. (e) ~ (g) and (h) ~ (j) are charge differences of Li adsorption at the edge site, sub-surface site and the bulk site relative to pristine graphite in armchair-edged and zigzag-edged systems, respectively. The iso-surface value is 0.001 e/Å^3.

Comparing the spin densities of these two systems provides further insights. The zigzag edge shows a completely different spin density distribution compared to the armchair edge (see Figure 1 a and b). Unpaired electrons accumulate on the carbon atoms of the zigzag edge. The character of these states is dominated by p_z orbitals perpendicular to the carbon basal plane. The amplitude of this topological surface state gradually diminishes over a few bond distances beneath the surface (see Figure 1d), which is in agreement with other reports.[44,45] It is this surface state that interacts with Li at the zigzag edge.

Figure 2 shows the local density of states (LDOSs) projected on the first layer of carbon hexagons near the armchair edge and zigzag edge, respectively. The armchair edge has the same semi-metallic character that characterizes the bulk: the DOS nearly decreases to zero at the Fermi energy while it shows significant contribution from the valence and conduction bands dominated by C 2*p* orbitals. The excess electron due to Li adsorption induces a slight shift of Fermi energy to higher energies, but not a qualitative change of the DOS character. Furthermore, the main peak of the Li 2*s* orbital occurs at a very high energy level (about 6 eV above the Fermi level as shown in Figure S4), although there is also a weaker broad feature with Li 2*s* character below the Fermi level. In addition, Bader charge analysis shows Li possessing a charge of +1|e|. This indicates a largely ionic character of the bonding between Li and adjacent carbons with some limited covalency.

The charge differences of Li adsorption on the edge sites and sites near the edge are shown at the bottom of Figure 2. In the armchair system, electron-transfer to the adjacent carbon atoms is similarly localised at the edge and sub-surface sites. But relative to the sub-surface sites, Li adsorption at the edge site results in a slightly larger charge transfer to the surrounding carbon atoms. This might explain the slightly increasing adsorption energy at the edge site, while the sub-surface sites effectively show bulk behaviour.

In the zigzag-edged system, the valence band and conduction band are also dominated by C 2*p* orbitals at the zigzag edge (see Figure 2 c and d). However, an additional state with p_z orbital character crosses the Fermi level according to the LDOSs in Figure 2c. This "peculiar" C surface state is a consequence of the zigzag topology as has been shown theoretically before for unsaturated graphite sheets.[27,46] That the same electronic state is observed here already indicates that it is relatively insensitive to the nature of the surface termination (as we have used a H terminated model). Hydrogen termination is attractive for theoretical studies because the formed σ-bond does not interact with the C p_z manifold,[28,44-47] but other surface terminations are likely to exist on the solid side of the solid electrolyte interphase (SEI).[48,49] It has been found that removing all oxygen functionality from the surface leads to unstable SEI formation.[48] Practical graphitic electrodes, therefore, likely show some functionalisation with oxygenated surface groups. Therefore, we also briefly explored other terminations such as hydroxyl groups (OH) and fluorine (F) to verify the relevance of conclusions from of our simple H-terminated model for battery applications. The topological surface state is also observed across the Fermi level with OH and

F terminated zigzag-edged graphite (see Figure S5). The concrete chemical nature of the σ-bonded, terminating groups, therefore, does not qualitatively change the phenomena.

Li adsorption also leads to a shift of the Fermi level to higher energies in the zigzag edged system. However, in contrast to the Fermi level shift after Li adsorption in the armchair system (0.14 eV), here the Fermi level only shifts by 0.06 eV because of the significant density of states due to the surface state around the Fermi level. The Li 2*s* projected DOS is very similar to that seen near the armchair edge with the main peak again appearing above the Fermi level, showing a similar ionic bonding character (see Figure S4b).

However, the character of the surface state changes markedly at the zigzag edge as can be seen by comparing the p_z-projected LDOSs in Figure 2c and d, respectively. The peak at 0.6 eV becomes sharper, while the band at -0.5 eV broadens. This suggests some electronic interactions between the surface state and Li (and/or its electron), which can be verified by charge difference analysis. Figure 2h shows the charge difference after Li adsorption at the zigzag edge. Charge transfer clearly occurs from Li to the surface state of edge carbons after Li adsorption on the edge site. But the charge transfer is less localised compared to the armchair edge with a significant transfer to the edge C atoms not surrounding the adsorption site. This electron transfer to surface C sites has not been observed near the armchair edge (see Figure 2e-g). Li donates the electron to zigzag edge and, therefore, fills the C surface state, which acts as an electron-acceptor.

A similar behaviour is found when Li adsorbs at a sub-surface site (see Figure 2i). Li also contributes electron density to the edge carbons, but the additional electron density at the edge becomes smaller with increasing distance from the edge. Simultaneously, the magnitude of the Li adsorption energy decreases gradually from -0.66 eV. When Li adsorbs sufficiently far away from the edge (about 4.3 Å) no visible electron density transfer between Li and the C surface state occurs (see Figure 2j), and the adsorption energy decreases to -0.38 eV. An analogous trend of decreasing Li adsorption energy from edge to bulk was found in OH and F terminated zigzag-edged graphite (as shown in Table S4 and Figure S5), indicating that this trend is not specific to H terminations. This reduced charge transfer to the surface with increasing distance of Li from the surface agrees well with the exponential decay of the spin density (cf. Figure 1),[31,46,50,51] and the gradual decrease of the Li adsorption energy, going from the edge to the bulk.

In summary, this peculiar electron-transfer mechanism near the zigzag edge strongly stabilizes Li adsorption near that edge. In other words, the topological C surface state at the zigzag edge can pin Li near the edges with a potentially detrimental impact on intercalation rates.

3.2 Li diffusion in edged graphite

Li diffusion near graphite edges and in the bulk is explored to quantify the edge effect on Li diffusion. Li diffusion possesses much lower energy barriers along the basal plane than through the hexagonal hollow of the carbon sheets in bulk graphite.[17,26] Therefore, we only consider Li diffusion along the basal plane.

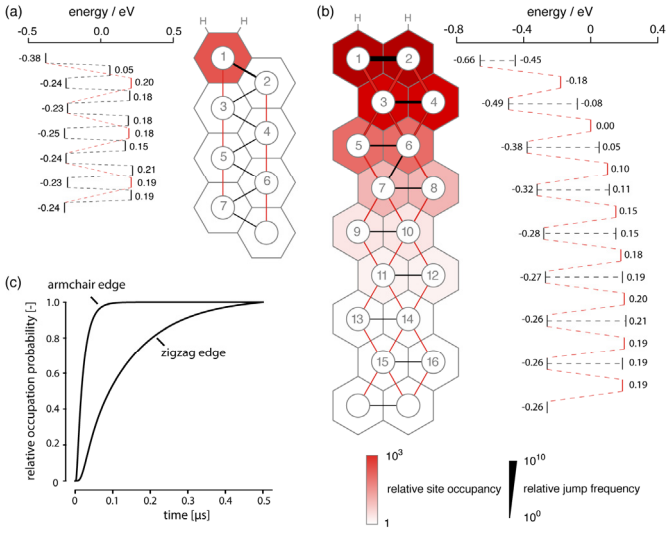

Figure 3. Li diffusion at (a) armchair-edged and (b) zigzag-edged graphite. Colored hexagons indicate site occupancy relative to bulk and the width of the lines connecting sites indicates jump frequency; (c) probability for Li to occupy a site approximately 20 Å below the surface relative to the steady-state value after being introduced at time zero at the edge.

Figure 3 shows the energetics of Li diffusion from the edge towards the bulk for both systems. The diffusion process complies with a hopping mechanism, in which Li hops from one hollow site to the adjacent hollow site by going across the carbon-carbon bridges, where the transition state is located. In armchair-edged graphite, two possible paths were identified for Li diffusion: (1) a “stepwise” mechanism (shown in black in Figure 3), where Li diffuses from site 1 to site 2 and then moves to site 3 before progressing towards the bulk, and (2) a “direct” pathway where Li jumps from site 1 to site 3 without hopping first to site 2 (shown in red in Figure 3) and then diffuses to the bulk. The energy profile shows that Li diffusion has lower individual jump barriers via the “stepwise” mechanism with barriers of 0.43 eV (site 1 to site 2) and 0.42 eV (site 2 to site 3). In contrast, a direct jump from site 1 to 3 must overcome an energy barrier of 0.58 eV. Away from the edge, the “direct” and “stepwise” mechanisms become competitive with similar energy barriers (e.g. 0.41 eV from site 3 to site 5; 0.40 and 0.39 eV from site 3 to site 5 via site 4) as symmetry would suggest. As the energy profile shows, the activation energies are not very sensitive towards the distance from the edge; they all are within ±0.05 eV of 0.2 eV with the transition from site 1 to 2 being the notable exception.

It is tempting to conclude that the stepwise mechanism is preferred on the grounds of lower individual activation energies. This, however, would ignore that two steps are needed to reach site 3 and that fluxes also depend on concentration as well as activation energies. In the dilute limit, Li jumps are uncorrelated, and a simplified Markov chain model can be used to estimate jump frequencies:

$$\mu^{t+1} = \mathbf{P}\mu^{t} \qquad (2)$$

where **P** is the matrix of transition probabilities and μ is the occupation probability for Li to occupy sites. The flux of Li from site *i* to site *j* is then given by $f_{ij} = \mu_i \mathbf{P}_{ij}$.

The right-hand side of Figure 3a visualises the results of a simplified Markov process near the armchair edge at room temperature that is described in more detail in the Supporting Information. Occupation probabilities are visualized by different shades of red (darker red equals higher probability) of the hexagons and steady-state fluxes are visualized by the thickness of lines connecting sites. Naturally, the lower site energy of site 1 leads to a higher occupancy of this site relative to other sites by a factor of approximately 2.7×10^2. This higher site occupancy has two consequences: (1) it over-compensates the higher activation energy to jump from site 1 to 2 (relative to the bulk) resulting in an increase of flux between these two surface sites of about 4×10^2 relative to bulk sites, and (2) it counterbalances the very substantial increase in activation energy to jump from site 1 to site 3 yielding similar fluxes as for jumps from site 2 to 3 (and between bulk sites). The energy landscape near the armchair edge, therefore, suggests that Li is more mobile within the edge sites, but it jumps with equal frequency into sites further away from the edge from either of the edge sites despite the differences in occupation probability between site 1 and 2.

In zigzag-edged graphite, there are also two possible paths for Li diffusion as shown in Figure 3b. In path 1, Li diffuses at the zigzag edge along the (010) direction (e.g. from site 1 to site 2 – black in Figure 3), whereas in path 2 Li moves perpendicular to the edge to reach bulk sites (e.g. diffusing from site 1 to site 3 and so on – red in Figure 3). The energy barrier of Li diffusion from the edge site 1 to the sub-surface site 3 is 0.48 eV, similar to perpendicular diffusion barriers further away from the edge and comparable to energy barriers seen for the armchair edge. However, Li diffusion along the edge sites only has to overcome an energy barrier as low as 0.21 eV at the surface. Li is, therefore, extremely mobile within these edge sites at the first layer below the surface. Even for the first sub-surface sites Li still prefers to diffuse along the (010) direction, because the activation barrier between site 3 and 4 is 0.41 eV and lower than for jumping further inside (0.49 eV) by 0.08 eV. Generally, the energy barriers for Li to diffuse along the (010) direction increase gradually and eventually reach bulk-like values. The stronger lines connecting sites in Figure 3b visualize the higher mobility near the edge. The logarithmic scale is worthwhile noting. The combination of higher average occupancy and lower activation barriers both contribute to the substantial increase of mobility.

Finally, Figure 3c shows the relative probability for Li to occupy a site approximately 20 Å beneath the armchair and zigzag surface after being introduced at the edge site at time zero as given by the recursion $\mu^{[t+1]} = \mathbf{P}\mu^{[t]}$ assuming an attempt frequency of 10^{13} Hz.[16] Despite broadly similar activation energies for jumps towards the bulk, Li exchange between the zigzag edge and bulk is much slower than the dynamics near the armchair edge. The time constant for Li to reach a steady-state distribution 20 Å below the zigzag edge is of the order of 1 µs at room temperature, while the same process below the armchair edge is at least one order of magnitude faster. This is a consequence of the strong stabilization of Li near the zigzag edge. Li has not only to overcome the individual activation barriers, it also has to "climb" out of the potential energy well that is a consequence of the interaction between Li and the topological surface state near the edge, which is a process involving several sites.

In summary, this detailed analysis of the dynamics near the armchair and the zigzag edges has shown that Li dynamics near the armchair edge are broadly similar to the bulk (except the topmost surface layer), but near the zigzag edge Li is more mobile within the surface plane, but also pinned there reducing the transfer rate to the bulk by at least one order of magnitude. This effect is much longer ranged and persists over approximately five to six atomic layers into the bulk. We, therefore, expect the (de)intercalation kinetics to be much more sluggish at the zigzag edge than the armchair edge.

3.3 Doping implication on Li intercalation

As Li pinning at the zigzag edge can be traced back to the electronic structure near the Fermi level, it is interesting to consider the impact of doping on Li energetics/dynamics near the edges. In graphene-related materials, chemical doping was widely investigated by both modelling and experiments, reporting advantages for enhancing charging or discharging of LIBs.[52-59] However, intentional doping of the surface, and particularly the distinction between armchair and zig-zag sites doped in this way, has hardly been explored.

Boron (B) and nitrogen (N) doping at graphite edges is attractive to modify the local electronic structure and tune the Li intercalation behaviour as both types of doped carbons are common, readily available experimentally, and relatively inexpensive.[52,53,55,56,58] We considered B (p-type) and N (n-type) doping at both graphite edges by replacing one of the edge carbons (see Figure 4).

Table 1. Li adsorption at the edges of pristine, N and B doped graphite. E_{Fermi} is the Fermi level relative to vacuum; ΔE_{Fermi} is the difference of Fermi levels between the pristine and doped graphite. E_{ads} is the Li adsorption energy as defined in equation (1).

Edges		E_{ads}/eV	E_{Fermi}/eV	ΔE_{Fermi}/eV
	N dope	-0.17	2.28	0.11
Armchair	Pristine	-0.38	2.17	0.00
	B dope	-0.89	1.94	-0.23
	N dope	-0.55	3.14	0.07
Zigzag	Pristine	-0.66	3.07	0.00
	B dope	-0.75	2.99	-0.08

Table 1 summarises the adsorption energies of Li under different types of doping. The Li adsorption energy reduces significantly to -0.17 eV in the N doped armchair system compared to pristine graphite (-0.38 eV). The B doped system, on the other hand, shows the opposite trend with the Li adsorption energy rising to -0.89 eV.

DOSs calculations of pristine, B- and N-doped armchair systems (see Figure S6) show markable differences in the electronic structure. First, the Fermi level shifts in the N- and B-doped systems: B-doped graphite shows a shift from 2.17 eV for pristine graphite to 1.94 eV. N doping on the graphite edge has the opposite effect: the Fermi level shifts from 2.17 to 2.28 eV.

To first approximation, these shifts in Fermi energy (relative to vacuum) can be understood in a band filling picture (although changes to surface dipoles might contribute as well). In comparison with pristine graphite, B doping provides one less electron while N doping will contribute one more electron to the system. Therefore, N-doped graphite becomes electron rich, occupying additional electronic states above the Fermi level of pristine graphite, while the B doped system is electron deficient, and therefore frees electronic states below the Fermi level of pristine graphite. The donated electron (hole), however, does not fully delocalize. There is a net positive additional charge density around the B doped site, whereas considerable additional negative charge density builds around the N doping site (cf. Figure 4a and b, respectively).

Since Li has weak covalent binding and shows mostly ionic bonding with surrounding carbon atoms, it can be considered as an electron donor. Accordingly, when Li adsorbs in the B-doped system, the electron from Li can "benefit" from the additional unoccupied states and reduced coulombic repulsion, thereby increasing the Li adsorption energy. In the N-doped system, the opposite is the case: the Fermi level accepting electrons has shifted to higher energies and the additional electron density near the adsorption site will lead to additional Coulomb repulsion, which decreases the Li adsorption energy.

A similar trend is seen for zigzag-edged graphite, but less pronounced. In terms of Li adsorption, the adsorption energy increases in magnitude to -0.75 eV in the B-doped system, while it reduces in magnitude to -0.55 eV in the N-doped system. Hence, both dopants seem less effective with respect to changing the adsorption energy than is observed for armchair-edged graphite. Doping N only reduces the adsorption energy by 0.11 eV which is smaller than the decrease in the armchair system of 0.21 eV; B doping only promotes the adsorption energy of Li by 0.09 eV, which is much smaller than the 0.51 eV increase seen in the armchair system.

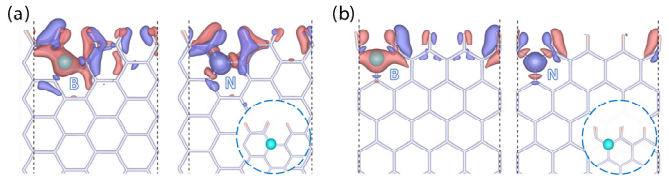

Figure 4. The charge difference of B/N doped graphite which is difference between the charge densities of doped graphite and pristine graphite. (a) and (b) are the charge differences of N and B doped system in armchair and zigzag edged systems, respectively. The inserted figures are corresponding geometries. The iso-surface value is 0.012 e/Å^3.

Similarly, the Fermi energy is less sensitive in the zigzag edged system. It only increases by 0.07 eV in the N-doped zigzag system and decreases by 0.08 eV in the B-doped system (see Figure S7). Finally, the charge transfer between the doping sites and graphite edges also becomes smaller than in the armchair system (see Figure 4b).

The DOS near the Fermi level is dominated by the additional topological surface state in the zigzag edged system, providing significant additional density of states near the Fermi energy. Hence, changes to the Fermi level due to doping are less pronounced and, in consequence, B and N doping have a smaller effect on Li adsorption energies in the zigzag system.

Whilst interpretation in a simple band filling picture is attractive and can explain trends, the localised changes to the charge density shown in Figure 4 suggest that doping creates a relatively localized effect. Hence, B and N doping further away from the edges (see Figure S8) of both systems was also considered to estimate effects on Li adsorption from dopants that are not directly adjacent to the adsorption site. In the armchair-edged system, the adsorption energies of Li at the edge site change to -0.58 and -0.34 eV, respectively, when B and N are doped at bulk-like sites with a distance between doping site and Li adsorption site of 7.79 Å. Both adsorption energies are closer to the value in pristine graphite (-0.38 eV) in contrast to the adsorption energies with doping at the edge (B doping: -0.89 and N doping: -0.17 eV). To be more specific, the adsorption energy approaches that of pristine graphite in the N-doped armchair system, implying a quite local effect of N doping. When doping B at a bulk-like site rather than the edged site, the Li adsorption energy decreases from -0.89 to -0.58 eV, but it is still more negative than that of pristine graphite by -0.20 eV. The effect of B doping on Li adsorption energies is, therefore, somewhat longer-ranged than N doping. In the zigzag system, Li adsorption energies also strongly depend on the distance between dopant and adsorption site. Li adsorption energies become -0.67 and -0.62 eV with B and N doping at a bulk-like site around 12.78 Å away from the adsorption site, which is close to the adsorption energy of Li at the edge site in pristine graphite (-0.67 eV).

It's worth noting that the change of Li adsorption energies is proportional to the Fermi energy shift. Figure 5 shows the relative Li adsorption energies ($\Delta E'_{ads}$) as a function of Fermi energy shift (ΔE_{Fermi}). $\Delta E'_{ads}$ and ΔE_{Fermi} is defined as:

$$\Delta E'_{ads} = \Delta E_{ads}(\text{Li|pristine graphite}) - \Delta E_{ads}(\text{Li|doped graphite}) \quad (3)$$

$$\Delta E_{Fermi} = E_{Fermi}(\text{doped graphite}) - E_{Fermi}(\text{pristine graphite}) \quad (4)$$

A good linear relationship between $\Delta E'_{ads}$ and ΔE_{Fermi} is observed. The correlation holds for bulk and edged graphite with B and N doping and can be rationalized with the simple band filling argument made earlier: B doping lowers the Fermi energy and hence increases the Li adsorption energy by providing lower energy acceptor states in the C p_z manifold. N doping has the opposite effect. Interestingly, the slope of the relation equals two for the armchair edge and bulk graphite

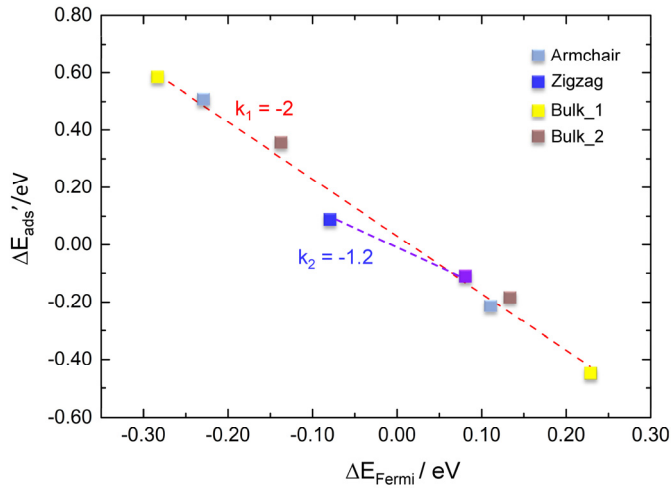

Figure 5. The linear relationship between the relative Li adsorption energy changes ($\Delta E_{ads}^{'}$) and Fermi energy shift (ΔE_{Fermi}) in edged and bulk graphite with B and N doping. k_1 and k_2 are the slopes of red and blue linear relations, respectively.

systems, meaning that an increase in Fermi energy leads to twice the decreasing in adsorption energy. This is attributed to the diamagnetic character of the system. Spin up and spin down states contribute equally to the density of states near the Fermi level. Hence, a shift of the Fermi energy affects the filling of both spin channels equally leading to twice the energy shift of the adsorption energy. The admittedly limited data for the zigzag edge, however, suggests a slope closer to one for zigzag edge system, implying that an increase in Fermi energy leads to an equivalent decrease in adsorption energy. This is attributed to the ferromagnetic magnetization property of the zigzag edge with only one spin channel contributing at the Fermi level at an edge.[44,45] Therefore, only one free spin channel can be filled by the electron, which gives a theoretical slope of one.

3.4 Implications for experimental validation

A possible strategy to experimentally study these edge effects would be to preferentially grow either edge through advanced synthesis followed by physical and electrochemical characterisation. For instance, Bernado et al. systematically controlled the proportion of these edges through preferential etching of graphite particles in oxygen or water vapour environments.[60] The focus of their study was on SEI formation and not intercalation dynamics. But they demonstrated different reactivity towards the electrolyte for these edges, and a similar experimental strategy can easily be envisioned to enable edge-resolved, kinetic intercalation studies as well.

The same synthesis methodologies could also be applied to materials for bespoke experiments to probe the difference in adsorption energy dependent on the proportion of different types of edge site. For example, Velicty et al. recently examined the local electron transfer rate, double layer capacitance and the density of states of the edge versus the basal plane in a microdroplet electrochemical cell.[61] The double layer capacitance is interpreted to be correlated with the density of states at the Fermi level,[62] and so, based on the present work, would also be expected to be related to the edge structure.

Direct experimental evidence of the topological surface state were found by Kluskek et al. and Koyashi et al. through scanning tunneling spectroscopy of hydrogen etched highly oriented pyrolytic graphite (HOPG) surfaces in non-electrochemical environments.[63,64] A surface state was identified between 90–250 meV and tentatively ascribed to the zigzag edge.[64] This prediction was validated by tight binding calculations of bilayer graphene.[63] Through a similar experimental approach, edges could be prepared with a different proportion of zigzag/armchair sites through control of the experimental conditions and through the use of different etchant gases and surface groups and then subjected to advanced characterisation techniques such as electrochemical STM or ambient pressure XPS to directly interrogate the electronic structure near the surfaces in electrochemical environments.

Theoretical trends identified here for surface boron and nitrogen doping agree with systematically controlled experimental bulk boron and nitrogen doping in graphite. Dahn et al. identified an increase (decrease) in lithium intercalation voltage in graphite with systematically increasing boron (nitrogen) doping, respectively.[65,66] This is in qualitative agreement with the role of boron (nitrogen) as an electron acceptor (donor), respectively. While doping of the basal plane has been explored, for example by Dresselhaus and co-workers, edge doping of bulk graphite in particular has not.[67] The controlled synthesis routes utilising HOPG outlined above followed by heat treatment with boron or nitrogen precursors could lead to lead to well-defined, doped non-basal plane surfaces that can be experimentally studied.

Alternatively, bottom-up synthesis approaches could be utilised to systematically modify graphite particles of controlled size. In particular, nitrogen hetero-atom doping of carbon nanostructures has been explored to rationally tune the interface;[68] more recently the use of other dopants such as boron has been explored.[52] Synthesis approaches explored so far include post treatment of carbon structures with reactive nitrogen,[69] pyrolysis or chemical vapour deposition with carbon and nitrogen/boron precursors,[66,67] or hydrothermal carbonisation.[68] So far, nitrogen doping work has focussed on evaluating structure-property relationships in electrocatalysis.[68,69] Similar methodologies could be applied to systematically investigate the intercalation behaviour as a function of boron or nitrogen surface concentration.

Finally, on the basis of the calculations performed here, the two types of edges could be distinguished by their differing magnetic properties. The principle has been demonstrated through the energy spectrum and dispersion in a magnetic field of zigzag nanoribbons.[70] Through careful study of the Pauli paramagnetic susceptibility, this approach could likewise be applied as a means to characterise the zigzag/armchair ratio in graphite particles with controlled basal to edge plane surface areas.[71,72]

4. Conclusions

The energetics and dynamics of Li intercalation near the non-basal edges of graphite have been investigated from First Principles. The unique electronic structure near the edges, particularly near the zigzag edge (i.e., a peculiar topological surface state), induces the following different Li adsorption and diffusion mechanisms at graphite edges compared to bulk at the dilute limit:

i) adsorption energies near the zigzag edge are much larger than in the bulk or near the armchair edge due to the surface state crossing the Fermi energy, which is energetically beneficial for Li to donate electrons to the host near the edge;

ii) Li mobility is direction-dependent at the zigzag edge and to a lesser degree at the armchair edge. Li jumping frequencies are higher parallel to the edges;

iii) activation energies for jumps towards the bulk are broadly similar for both edges and comparable to bulk (~0.5 eV at edge sites vs ~0.43 eV at bulk sites), but Li nonetheless intercalates much more readily into graphite through armchair edges than zigzag edges at dilute concentrations because of the "pinning" effect of the topological surface state;

iv) both B and N doping have considerable influences on the energetics of Li adsorption at the armchair edge and to a lesser degree at the zigzag edge, which can be rationalized to first approximation in a band filling picture.

We conclude that edge effects have considerable bearings on Li intercalation into graphite but have not attracted enough attention so far. The differences between the zigzag and armchair edge might provide opportunities to tailor carbons for higher rate (especially at low temperatures) by promoting armchair edges over zigzag edges. Further, the strong stabilization of Li near the zigzag edge could be a precursor for dendrites. Hence, reducing the prominence and/or changing the electronic structure of zigzag edges could also have implications on durability. Similarly, doping with N or B could be a promising avenue to tailor interface properties with a view to enhancing rate and durability. Finally, a better understanding of these edge effects might provide new rational design approaches for tailored, artificial Solid-Electrolyte-Interphases (SEIs). For instance, the large in-plane mobility near the zigzag edge could allow for SEIs with less permeable parts by relying on the large in plane mobility to effectively distribute Li on the solid side of the interface and promote homogeneous intercalation.

Conflicts of interest

There are no conflicts to declare.

Acknowledgements

The authors acknowledge the financial support from the Faraday Institution and EPSRC (faraday.ac.uk; EP/S003053/1), grant number FIRG003. We are grateful to the Iridis5 Supercomputer of the University of Southampton, the Michael Supercomputer of the Faraday Institution and the UK Materials and Molecular Modelling Hub for computational resources, which is partially funded by EPSRC (EP/P020194/1).

References

1 M. Li; J. Lu; Z. Chen; K. Amine. *Adv. Mater.* 2018, **30**, 1800561.
2 V. Etacheri; R. Marom; R. Elazari; G. Salitra; D. Aurbach. *Energy Environ. Sci.* 2011, **4**, 3243-3262.
3 J. B. Goodenough; Y. Kim. *Chem. Mater.* 2010, **22**, 587-603.
4 M. S. Whittingham. *Chem. Rev.* 2004, **104**, 4271-4302.
5 L. Ji; Z. Lin; M. Alcoutlabi; X. Zhang. *Energy Environ. Sci.* 2011, **4**, 2682-2699.
6 J. M. Tarascon; M. Armand. *Nature* 2001, **414**, 359-367.
7 W. Rüdorff; U. Hofmann. *Z. Anorg. Allg. Chem.* 1938, **238**, 1-50.
8 A. Yoshino. *Angew. Chem. Int. Ed.* 2012, **51**, 5798-5800.
9 D. Guerard; A. Herold. *Carbon* 1975, **13**, 337-345.
10 J. O. Besenhard; H. P. Fritz. *Angew. Chem. Int. Ed.* 1983, **22**, 950-975.
11 S. Konar; U. Häusserman; G. Svensson. *Chem. Mater.* 2015, **27**, 2566-2575.
12 M. Drüe; M. Seyring; M. Rettenmayr. *J. Power Sources* 2017, **353**, 58-66.
13 E. M. Gavilán-Arriazu; O. A. Pinto; B. A. López de Mishima; D. E. Barraco; O. A. Oviedo; E. P. M. Leiva. *Electrochem. Commun.* 2018, **93**, 133-137.
14 R. Yazami; Y. Reynier. *J. Power Sources* 2006, **153**, 312-318.
15 H. He; C. Huang; C.-W. Luo; J.-J. Liu; Z.-S. Chao. *Electrochim. Acta* 2013, **92**, 148-152.
16 K. Persson; V. A. Sethuraman; L. J. Hardwick; Y. Hinuma; Y. S. Meng; A. Van Der Ven; V. Srinivasan; R. Kostecki; G. Ceder. *J. Phys. Chem. Lett.* 2010, **1**, 1176-1180.
17 S. Thinius; M. M. Islam; P. Heitjans; T. Bredow. *J. Phys. Chem. C* 2014, **118**, 2273-2280.
18 K. Persson; Y. Hinuma; Y. S. Meng; A. Van der Ven; G. Ceder. *Phys. Rev. B* 2010, **82**, 125416.
19 K. Toyoura; Y. Koyama; A. Kuwabara; F. Oba; I. Tanaka. *Phys. Rev. B* 2008, **78**, 214303.
20 K. Toyoura; Y. Koyama; A. Kuwabara; I. Tanaka. *J. Phys. Chem. C* 2010, **114**, 2375-2379.
21 P. Yu; B. N. Popov; J. A. Ritter; R. E. White. *J. Electrochem. Soc.* 1999, **146**, 8-14.
22 H. Yang; H. J. Bang; J. Prakash. *J. Electrochem. Soc.* 2004, **151**, A1247-A1250.
23 N. Takami; A. Satoh; M. Hara; T. Ohsaki. *J. Electrochem. Soc.* 1995, **142**, 371-379.
24 M. Petzl; M. Kasper; M. A. Danzer. *J. Power Sources* 2015, **275**, 799-807.
25 J. Vetter; P. Novák; M. R. Wagner; C. Veit; K. C. Möller; J. O. Besenhard; M. Winter; M. Wohlfahrt-Mehrens; C. Vogler; A. Hammouche. *J. Power Sources* 2005, **147**, 269-281.
26 Q. Liu; S. Li; S. Wang; X. Zhang; S. Zhou; Y. Bai; J. Zheng; X. Lu. *J. Phys. Chem. Lett.* 2018, **9**, 5567-5573.
27 E. G. Leggesse; C.-L. Chen; J.-C. Jiang. *Carbon* 2016, **103**, 209-216.
28 C. Uthaisar; V. Barone. *Nano Lett.* 2010, **10**, 2838-2842.
29 J. Zheng; Z. Ren; P. Guo; L. Fang; J. Fan. *Appl. Surf. Sci.* 2011, **258**, 1651-1655.
30 A. M. Garay-Tapia; A. H. Romero; V. Barone. *J. Chem. Theory Comput.* 2012, **8**, 1064-1071.
31 F. Valencia; A. H. Romero; F. Ancilotto; P. L. Silvestrelli. *J. Phys. Chem. B* 2006, **110**, 14832-14841.
32 A. Van der Ven; J. Bhattacharya; A. A. Belak. *Acc. Chem. Res.* 2013,

46, 1216-1225.
33 H. C. Yu; C. Ling; J. Bhattacharya; J. C. Thomas; K. Thornton; A. Van der Ven. *Energy Environ. Sci.* 2014, **7**, 1760-1768.
34 J. P. Perdew; K. Burke; M. Ernzerhof. *Phys. Rev. Lett.* 1996, **77**, 3865-3868.
35 G. Kresse; J. Furthmüller. *Comput. Mater. Sci.* 1996, **6**, 15-50.
36 G. Kresse; J. Hafner. *Phys. Rev. B* 1994, **49**, 14251-14269.
37 G. Kresse; D. Joubert. *Phys. Rev. B* 1999, **59**, 1758-1775.
38 P. E. Blöchl; O. Jepsen; O. K. Andersen. *Phys. Rev. B* 1994, **49**, 16223-16233.
39 G. Henkelman; H. Jónsson. *J. Chem. Phys.* 2000, **113**, 9978-9985.
40 G. Henkelman; B. P. Uberuaga; H. Jónsson. *J. Chem. Phys.* 2000, **113**, 9901-9904.
41 S. Grimme; S. Ehrlich; L. Goerigk. *J. Comput. Chem.* 2011, **32**, 1456-1465.
42 S. Grimme; J. Antony; S. Ehrlich; H. Krieg. *J. Chem. Phys.* 2010, **132**, 154104.
43 V. V. Avdeev; A. P. Savchenkova; L. A. Monyakina; I. V. Nikol'skaya; A. V. Khvostov. *J. Phys. Chem. Solids* 1996, **57**, 947-949.
44 H. Lee; Y.-W. Son; N. Park; S. Han; J. Yu. *Phys. Rev. B* 2005, **72**, 174431.
45 G. Lee; K. Cho. *Phys. Rev. B* 2009, **79**, 165440.
46 M. Fujita; K. Wakabayashi; K. Nakada; K. Kusakabe. *J. Phys. Soc. Jpn.* 1996, **65**, 1920-1923.
47 M. R. Mananghaya; G. N. Santos; D. Yu; C. Stampfl. *Sci. Rep.* 2017, **7**, 15727.
48 S. H. Ng; C. Vix-Guterl; P. Bernardo; N. Tran; J. Ufheil; H. Buqa; J. Dentzer; R. Gadiou; M. E. Spahr; D. Goers; P. Novák. *Carbon* 2009, **47**, 705-712.
49 H. Buqa; A. Würsig; J. Vetter; M. E. Spahr; F. Krumeich; P. Novák. *J. Power Sources* 2006, **153**, 385-390.
50 D. P. DiVincenzo; E. J. Mele. *Phys. Rev. B* 1984, **29**, 1685-1694.
51 M. P. Mercer; M. Otero; M. Ferrer-Huerta; A. Sigal; D. E. Barraco; H. E. Hoster; E. P. M. Leiva. *Electrochim. Acta* 2019, **324**, 134774.
52 D. H. Wu; Y. F. Li; Z. Zhou. *Theor. Chem. Acc.* 2011, **130**, 209-213.
53 T. Kondo; S. Casolo; T. Suzuki; T. Shikano; M. Sakurai; Y. Harada; M. Saito; M. Oshima; M. I. Trioni; G. F. Tantardini; J. Nakamura. *Phys. Rev. B* 2012, **86**, 035436.
54 X.-k. Kong; Q.-w. Chen. *Phys. Chem. Chem. Phys.* 2013, **15**, 12982-12987.
55 J. P. Paraknowitsch; A. Thomas. *Energy Environ. Sci.* 2013, **6**, 2839-2855.
56 M. D. Bhatt; C. O'Dwyer. *Phys. Chem. Chem. Phys.* 2015, **17**, 4799-4844.
57 D. Wang; J. Zhou; J. Li; Y. Wang; L. Hou; F. Gao. *ACS Sustain. Chem. Eng.* 2018, **6**, 7339-7345.
58 C. Kim; T. Fujino; T. Hayashi; M. Endo; M. S. Dresselhaus. *J. Electrochem. Soc.* 2000, **147**, 1265-1270.
59 J. R. Dahn; J. N. Reimers; A. K. Sleigh; T. Tiedje. *Phys. Rev. B* 1992, **45**, 3773-3777.
60 P. Bernardo; J. M. Le Meins; L. Vidal; J. Dentzer; R. Gadiou; W. Märkle; P. Novák; M. E. Spahr; C. Vix-Guterl. *Carbon* 2015, **91**, 458-467.
61 M. Velický; P. S. Toth; C. R. Woods; K. S. Novoselov; R. A. W. Dryfe. *J. Phys. Chem. C* 2019, **123**, 11677-11685.
62 H. Gerischer. *J. Phys. Chem.* 1985, **89**, 4249-4251.
63 Y. Kobayashi; K.-i. Fukui; T. Enoki; K. Kusakabe; Y. Kaburagi. *Phys. Rev. B* 2005, **71**, 193406.
64 Z. Klusek; Z. Waqar; E. A. Denisov; T. N. Kompaniets; I. V. Makarenko; A. N. Titkov; A. S. Bhatti. *Appl. Surf. Sci.* 2000, **161**, 508-514.
65 W. J. Weydanz; B. M. Way; T. v. Buuren; J. R. Dahn. *J. Electrochem. Soc.* 1994, **141**, 900.
66 B. M. Way; J. R. Dahn. *J. Electrochem. Soc.* 1994, **141**, 907-912.
67 M. Endo; T. Hayashi; S.-H. Hong; T. Enoki; M. S. Dresselhaus. *J. Appl. Phys.* 2001, **90**, 5670-5674.
68 M. Qiao; M.-M. Titirici. *Chem. Eur. J.* 2018, **24**, 18374-18384.
69 R. A. Sidik; A. B. Anderson; N. P. Subramanian; S. P. Kumaraguru; B. N. Popov. *J. Phys. Chem. B* 2006, **110**, 1787-1793.
70 K. Wakabayashi; M. Fujita; H. Ajiki; M. Sigrist. *Phys. Rev. B* 1999, **59**, 8271-8282.
71 J. P. Olivier; M. Winter. *J. Power Sources* 2001, **97-98**, 151-155.
72 K. Zaghib; G. Nadeau; K. Kinoshita. *J. Electrochem. Soc.* 2000, **147**, 2110.